TÜBİTAK

Turkish Journal of Electrical Engineering & Computer Sciences

http://journals.tubitak.gov.tr/elektrik/

Research Article

Turk J Elec Eng & Comp Sci
(2013) 21: 1 – 25

doi:10.3906/elk-1101-996

Artificial immunity-based induction motor bearing fault diagnosis

Hakan ÇALIŞ[1,*], **Abdülkadir ÇAKIR**[1], **Emre DANDIL**[2]
[1]Department of Electrical Electronic Engineering, Faculty of Technology,
Süleyman Demirel University, Isparta, Turkey
[2]Department of Computer Technology and Programming Education Program,
Vocational School of Higher Education, Bilecik University, Bilecik, Turkey

Received: 11.01.2011 • **Accepted:** 22.09.2011 • **Published Online:** 27.12.2012 • **Printed:** 28.01.2013

Abstract: In this study, the artificial immunity of the negative selection algorithm is used for bearing fault detection. It is implemented in MATLAB-based graphical user interface software. The developed software uses amplitudes of the vibration signal in the time and frequency domains. Outer, inner, and ball defects in the bearings of the induction motor are detected by anomaly monitoring. The time instants of the fault occurrence and fault level are determined according to the number of activated detectors. Anomaly detection in the frequency domain is implemented by monitoring the fault indicator bearing frequencies and harmonics, calculated using the bearing dimensions and number of rotor revolutions. Due to the constant fault location and closeness to the accelerometer, the outer race fault in the bearing is the easiest fault type to determine. However, the most difficult fault type to detect is the ball defect. By verification of the detection results, the motor load has very little effect on the fault.

Key words: Induction motor, fault diagnosis, bearing defects, artificial immunity, negative selection algorithm

1. Introduction

In industry, induction motors are the most widely used electromechanical energy conversion devices. Due to their low cost, robustness, and reliability, they are the preferred choice in various applications. However, due to working conditions such as humidity, dust, temperature, and lack of lubrication, the most worn parts, the bearings, cause faults in different parts of the motor. Induction motor faults are detected using temperature, vibration monitoring, bearing oil, and motor current signal analyzing techniques. Fault detection and the classification of induction motors are conventionally implemented by comparing the signal spectrum in the case of healthy and faulty conditions.

The most commonly encountered faults in induction motors are classified as the following [1]:

- Stator winding faults,
- Broken rotor bar or cracked rotor bar or end-rings,
- Static and dynamic air-gap irregularities,
- Bent shaft,
- Bearing faults,
- Axial misalignment and mechanical unbalances.

*Correspondence: calis@tef.sdu.edu.tr

Bearings, composed of inner and outer balls and cage, are used to support the rotor and shaft for free rotation in the air gap. In Figure 1, it is seen that bearing faults are the most common faults. Fault-indicating frequency components are monitored in the vibration signal spectrum.

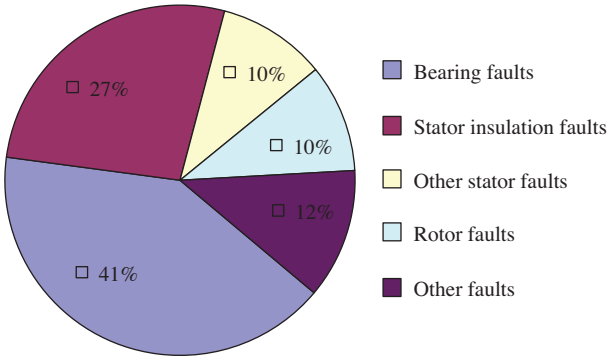

Figure 1. Faults and the fault rates in the induction motor.

Currently, advanced signal processing-based intelligent fault detection methods such as fuzzy logic, artificial neural networks (ANNs), the genetic algorithm (GA), the support vector machine (SVM) algorithm, and the data mining process are preferred for the early detection of motor faults. Gao and Ovaska [2] suggested that some of the soft computing methods should be used together.

Ayaz and Şeker [3] proposed the use of wavelet and statistical analyzing of vibration and motor current signals together for bearing fault detection in the induction motor. They defined the coherence function and determined misalignment faults by monitoring the fault indicator component using an ANN. ANN outputs are applied to the GA to find the maximum change on the bearing fault indicator component.

Orhan et al. [4] used a vibration analyzing technique to determine bearing faults. They stated that the easily detected bearing fault, particularly on the cylindrical rolling element bearing, is an outer race fault.

Özgönenel and Yalçın [5] implemented a study based on principal component analysis (PCA) combined with a feed-forward back-propagation neural network algorithm to detect stator winding, broken rotor bar, and bearing faults. This hybrid condition monitoring algorithm is based on a 3-phase supply current. They are preprocessed by the PCA to extract distinctive features. The neural network-based decision making then denotes a winding fault, rotor bar fault, bearing fault, and normal operation.

Kıral and Karagülle [6] proposed a finite element analyzing program for the case of multilocal defects, considering the load distribution, bearing geometry, and specifications. Vibration responses are analyzed under single or multilocal defects for different shaft speeds in both the time and frequency domains.

Costa Branco et al. [7] had concerns about the detection of broken bars, oscillator load, and unbalanced power supply faults in induction motors using immunology principles with motor current signal analysis. They were able to detect anomaly conditions at an early development stage using an immunity-based system.

Alataş et al. [8] proposed the use of a negative selection algorithm (NSA)-based immunity system for the detection of broken bars in induction motors. The increasing number of activated detectors and the number of frequencies at which each detector was activated was suggested for finding the fault type and level.

Abbasion et al. [1] investigated a method for multifault diagnosis based on wavelet denoising and a SVM algorithm. This investigation provided a procedure for the fault classification of rolling bearings using the SVM classifier.

Aydın et al. [9] detected broken rotor bars and stator short circuit faults and classified them using an artificial immunity-based SVM. The future vector is constructed based on Park's vector approach. The number of broken rotor bars and the level of stator winding faults were determined successfully.

Duan et al. [10] proposed a bearing and rotor fault diagnosis system by combining a NSA and immune network model. The diagnosis results showed that the abnormity degree increases when the fault becomes severe.

Aydın et al. [11] proposed detection of broken rotor bar faults using an artificial immune system (AIS) based on a NSA. Fault-related features were obtained using the Hilbert transform and the first difference filtering of a single-phase motor current. They used the GA to generate and optimize the detectors of the negative selection.

Gan et al. [12] used clonal selection programming (CSP) for a broken bar and voltage supply unbalance detection system in induction machines. The CSP-based classifier was used for fault identification and the classification of machine vibration signals obtained at different rotating speeds.

Martins et al. [13] presented an immune-based approach and a formal language algorithm for the detection of broken bars using a motor current signal. The increasing number of activated detectors revealed an abnormal machine condition.

Laurentys et al. [14] proposed a methodology to determine the difference between normal and abnormal conditions for DC motor fault detection based on an AIS using multioperational and negative selection algorithms.

Aydın et al. [15] proposed a chaotic-based hybrid NSA for broken rotor bar fault detection.

In this study, the AIS of the NSA is used for bearing fault detection. Outer, inner, and ball defects in the bearings of an induction motor are detected by anomaly monitoring. It is implemented in a MATLAB-based graphical user interface software. The developed software uses amplitudes of the vibration signal in the time and frequency domains. It distinguishes normal data from abnormal data. The fault diagnosis system is based on distance and similarity measurements implemented by a matching rule.

The rest of this paper is arranged as follows: in Section 2, we briefly describe the experimental setup, bearing geometry, and calculation of bearing defect frequencies; in Section 3, the artificial immunity-based fault diagnosis system and developed software are detailed; in Section 4, the experimental results are discussed; and, finally, conclusions are given in Section 5.

2. Experimental setup

All of the data related to the bearings and the system under investigation belong to the Case Western Reserve University Bearing Data Center [16]. The experimental setup is shown in Figure 2. It consists of a 2-hp, 3-phase induction motor; a dynamometer; and a torque sensor. The test bearings support the motor shaft. The dynamometer is adjustable to produce the desired torque load levels.

Bearing faults were introduced using electric discharge machining (EDM) with faults ranging from 0.0178 cm to 0.1016 cm in diameter separately at the inner race, rolling element, and outer race. Vibration data, from both the drive end and the fan end side, were collected with accelerometers when the bearings were normal and after faulted bearings were reinstalled in the test motor. They were recorded under the different motor loads. Accelerometers with a bandwidth of up to 5000 Hz and an output of 1 V/g were used to acquire the vibration signals from the bearings. The data were collected after being amplified at a sampling frequency of 12,000 Hz per channel. An antialiasing filter with a 5-kHz cut-off frequency was used prior the sampling. Drive end and

fan end bearing specifications are given in Table 1. The bearing geometry is shown in Figure 3.

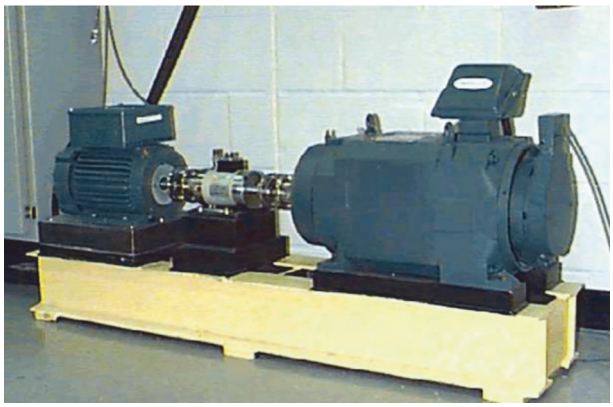

Figure 2. Induction motor test experimental setup [16].

Table 1. Bearings specifications, including bearing geometry and defect frequencies.

Location of bearing		Drive end	
Type of bearing		6205-2RS JEM SKF	
Size	Value (cm)	Defect frequencies	Multiple of running speed
Inside diameter	2.5001	Inner race (f_i)	5.4152
Outside diameter	5.1999	Outer race (f_o)	3.5848
Ball diameter (D_b)	0.7940	Rolling element (f_b)	4.7135
Pitch diameter (D_p)	3.9040	Cage train (f_c)	0.3983
Thickness	1.5001		
Location of bearing		Fan-end	
Type of bearing		6203-2RS JEM SKF	
Size	Value (cm)	Defect frequencies	Multiple of running speed
Inside diameter	1.7000	Inner race (f_i)	4.9469
Outside diameter	3.9999	Outer race (f_o)	3.0530
Ball diameter	0.6746	Rolling element (f_b)	3.9874
Pitch diameter	2.8498	Cage train (f_c)	0.3817
Thickness	1.1999		

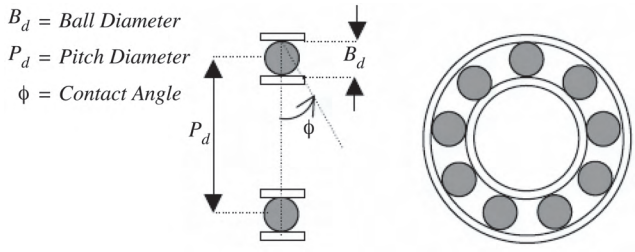

Figure 3. Bearing geometry [17].

The bearings generate 5 fundamental frequencies during the induction motor cycle. These are the inner race frequency (*fi*), outer race frequency (*fo*), fundamental cage frequency (*fc*), and rolling element frequency (*fb*). Defect frequencies are calculated using Eqs. (1) through (5), where d is the rotor speed (rpm), *fs* is the rotor speed (revolutions per second), and N is the number of balls. *Bd* is the ball diameter, *Pd* is the pitch

diameter, and θ is the bearing contingence angle.

$$f_s = d/60 \tag{1}$$

$$f_i = \frac{N}{2\left(1+\left(\frac{B_d}{P_d}\right)Cos\,\theta\right)} f_s \tag{2}$$

$$f_o = \frac{N}{2\left(1-\left(\frac{B_d}{P_d}\right)Cos\,\theta\right)} f_s \tag{3}$$

$$f_c = \frac{f_s}{2}(1-\frac{B_d}{P_d}Cos\,\theta) \tag{4}$$

$$f_b = \left(\frac{P_d}{2B_d}\right)\left(1-\left(\frac{B_d}{P_d}\right)^2 Cos^2\,\theta\right) f_s \tag{5}$$

A block diagram of the fault diagnosis system is shown in Figure 4. Vibration data are windowed before applying the AIS algorithm. Experimental data are investigated in both the time and frequency domains for fault diagnosis with the aid of the MATLAB-based graphic user interface.

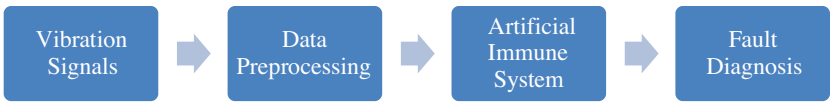

Figure 4. Block diagram of the system.

3. Artificial immunity-based fault diagnosis system

Immune systems have a complex structure with the capability of learning, memory, and novelty detection characteristics. This system protects our body against foreign cells called antigens. These antigens are recognized and eliminated by a process that is known as the immune response [18]. The fault detection approach used in this paper is inspired by the properties of natural immune systems. Immune systems have been applied to fault diagnosis, pattern recognition, anomaly detection, classification, and so on. Our fault detection algorithm is based on the discrimination of normal system patterns from any abnormal deviations. Commonly used AISs are composed of negative and clonal selection. While negative selection is applied to anomaly detection problems, clonal selection is used for optimization problems. In the training stage of the NSA, only self samples are given to the system, and appropriate detectors are generated [19].

In this context, AISs [20] are defined as a new computational paradigm based on metaphors of biological immune systems. In this paper, the NSA of artificial immunity is used for bearing fault diagnosis.

3.1. Negative selection algorithm

The NSA, inspired by negative selection, was prepared for change/anomaly detection by Forrest et al. [21]. This algorithm has some detectors, which can detect abnormal data. Various NSAs are proposed and characterized by particular representation schemes, matching rules, and detector generation processes [19]. In the generation stage, the candidate detector is produced at random and tested to see whether it recognizes the self samples. A detector that recognizes any sample is removed. Only those that cannot recognize self samples at all are added

to the detector set. In the detection stage, the input data are tested to see whether they are recognized by the detector set. This algorithm determines that the recognized data are abnormal and the unrecognized data are normal. The approach discussed here is based on the self/nonself discrimination capability. The basic principle from a computational perspective is as follows [22]:

- The self set is defined as a normal pattern of activity that needs to be monitored.
- The detector set, each of which fails to match any string in the self set, is generated. A matching rule is used, in which 2 strings match if and only if they are identical in at least r contiguous positions, where r is a suitably chosen parameter.
- New observations for changes are monitored by continually matching the detectors against the representative of the self set. Whenever any detector matches, it means that a change has occurred in the system behavior.

Figure 5 shows the detector generation and anomaly detection stages of the NSA.

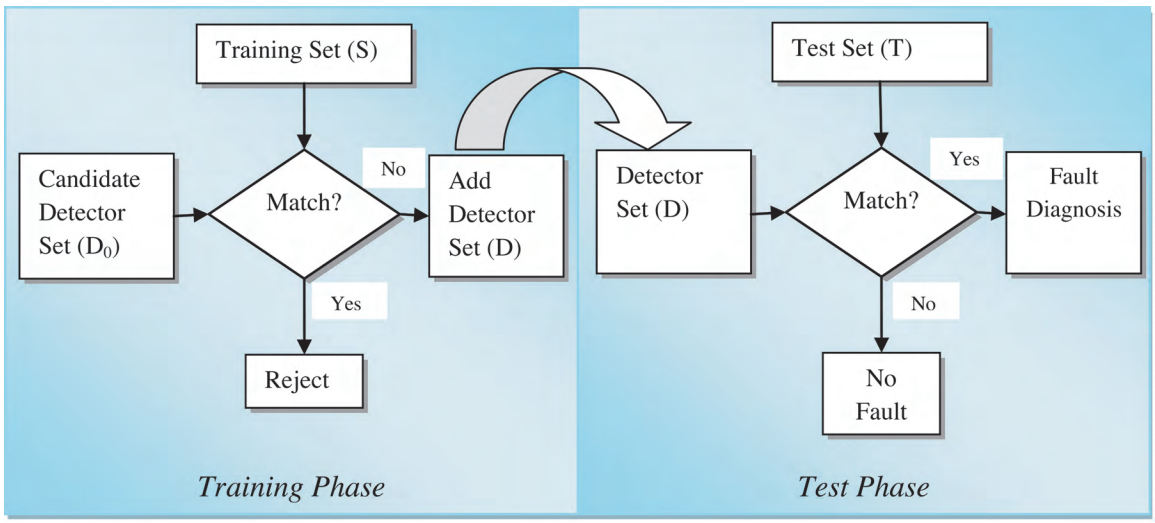

Figure 5. Negative selection algorithm of artificial immune system.

The steps of the NSA are as follows:

i. The first step is the determination of the training set (S: self set).

ii. Next is the random generation of candidate detectors (D_0: candidate detector set).

iii. This is followed by generation of a set of detectors that failed to match in S. In the matching rule, a match occurs between 2 patterns when their Euclidean distance (A) is less than the threshold (ε). In this case, this candidate detector is rejected and the process begins to generate another one. This loop continues until the defined number of detectors is completed. This produces a real detector set, which is known as the training stage (D: detector set).

iv. The first step in the test stage is the determination of the test set (T: nonself set).

v. In this step, there is an attempt to match the data in the detector set (D) with the data in the test set (T) according to the Euclidean distance and the ε (threshold). Any matched case indicates an abnormality; a lack of matches signifies a normal condition. The test stage is completed in this manner.

vi. In the final step, the results of the test stage are monitored.

The Euclidean distance used in the above steps is calculated as shown in Eq. (6).

$$A = \sqrt{\sum_{i=1}^{l} (Ab_i - Ag_i)^2} A = \sqrt{\sum_{i=1}^{l} (Ab_i - Ag_i)^2} \tag{6}$$

Here, Ab = [Ab_1, Ab_2,..., Ab_l] is the antibody set (i.e. the self set) and Ag = [Ag_1, Ag_2, ..., Ag_l] is the antigen set (i.e. the nonself set). The difference (E) between A and the threshold (ε) is calculated as shown in Eq. (7).

$$E = A - \varepsilon \tag{7}$$

If $E>$, the antigen set is not matched with an antibody set and it is added to the detector set. After a certain number of detectors are generated, they are used in the test stage to identify those not matched in the self set.

3.2. Description of the fault diagnosis software

In this paper, software has been developed using the principles of the NSA, and this software is used to diagnose faults in the inner race, outer race, and rolling element parts of induction motor bearings. The developed software, shown in Figure 6, consists of 2 divisions, fault diagnosis in the time and the frequency domains, which are activated by clicking the related button in the user interface.

The first phase of fault diagnosis is the determination of the training and test data, which are then loaded. Using all of the saved data from the accelerometer increases the computation time. Therefore, the amount of data is limited by selecting the window length and window key in the fault diagnosis software.

3.2.1. Fault diagnosis system in the time domain

Vibration signals obtained from healthy and faulty bearings are applied as input data for the NSA-based fault diagnosis system. The main idea of the fault diagnosis is based on finding the abnormal data above a certain threshold.

The appearance of the user interface system in the time domain is shown in Figure 8. In this part, the selection of a suitable window size, load level, and data type and other adjustments are done.

Fault diagnosis in the time domain is implemented in sequential steps. First, the data for both a healthy machine and a machine with faulty bearing are loaded, and then the location of the data file, window size, and fault position are selected. After all of the data are displayed in the time domain, an AIS-based fault detection algorithm is executed. In the graphic user interface, the fault level, number of activated detectors, and other related messages are displayed. Programming steps in the time domain algorithm are shown in Figure 9.

3.2.2. Fault diagnosis system in the frequency domain

In this section, the vibration data are analyzed in the frequency domain, particularly to find amplitude changes in the fault indicator components. Conversion of the time domain signal to the frequency domain is implemented

by Fourier transformation. Only bearing characteristic frequencies, related to bearing dimensions and motor speed, and their harmonics are monitored. They are fed into the NSA-based fault detection software as input data and any change above the determined threshold value is assumed as an abnormality for fault detection.

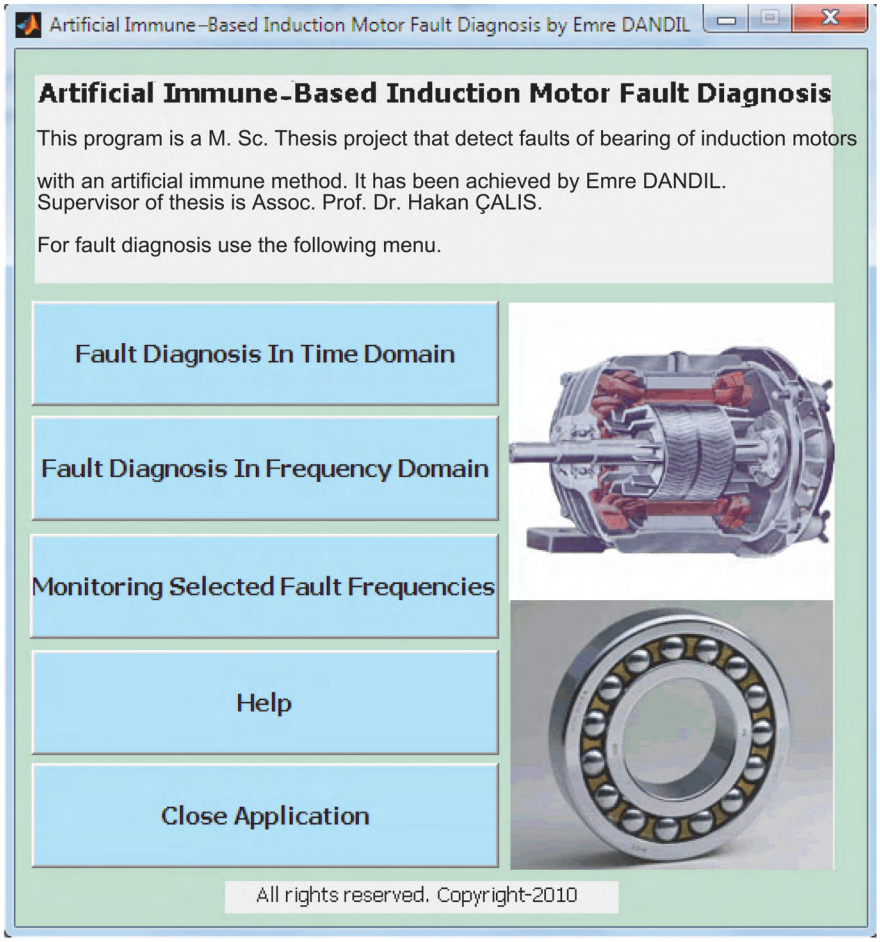

Figure 6. The graphical user interface of the main diagnostic software.

When the frequency domain is selected as in Figure 6, the result is the display in Figure 10. After you select the data, such as load level, fault type, harmonics, and other adjustments, execution of the fault detection algorithm begins in the frequency domain.

A flowchart of the bearing fault detection system in the frequency domain and the application steps are shown in Figure 11.

4. Experimental results

4.1. Results in the time domain

4.1.1. Diagnosis of bearing faults in the outer race

For outer race fault detection, first the training data are loaded, followed by the test data, and their details are displayed as in Figure 12. Here, the length of the window for the training and test data is defined as 416. This value is equal to the number of data to cover one complete cycle of motor rotation.

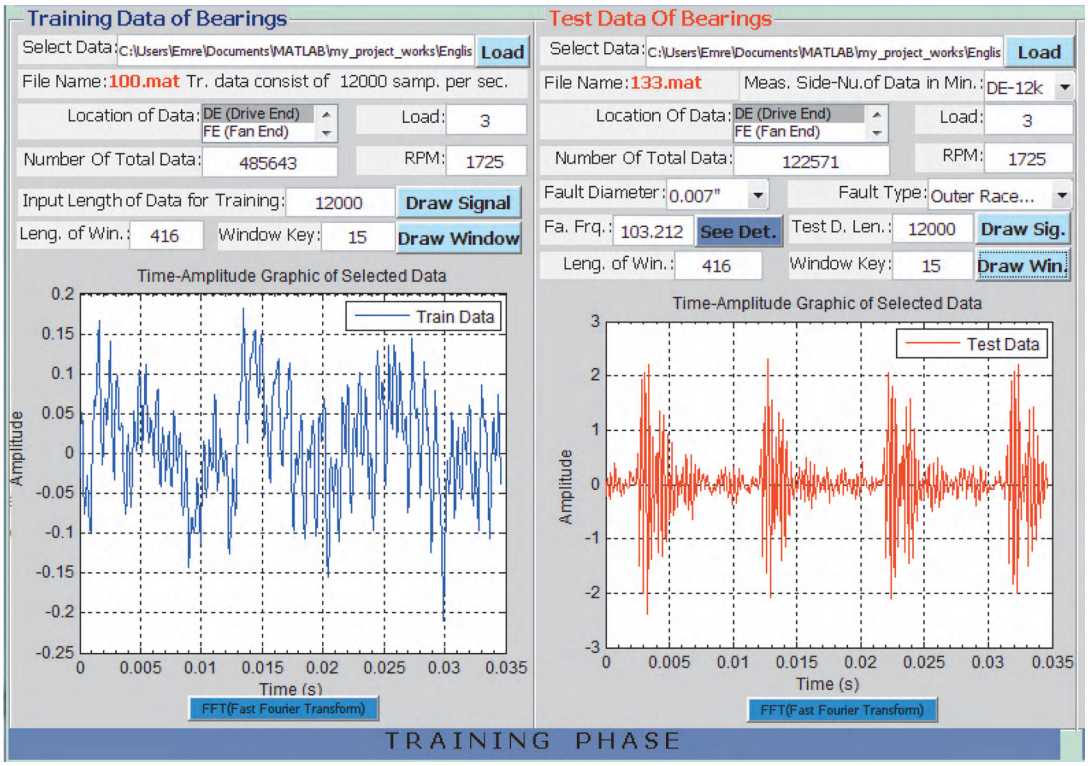

Figure 7. Determination of the test and training data.

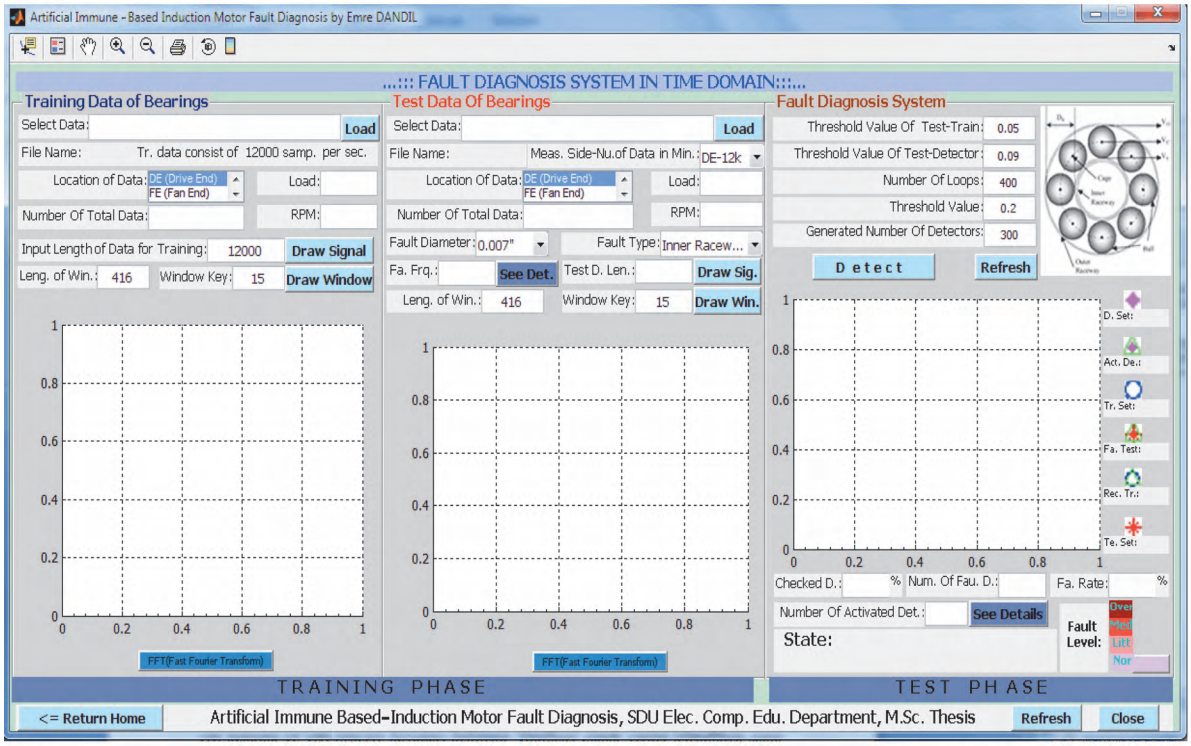

Figure 8. The fault diagnosis system in the time domain.

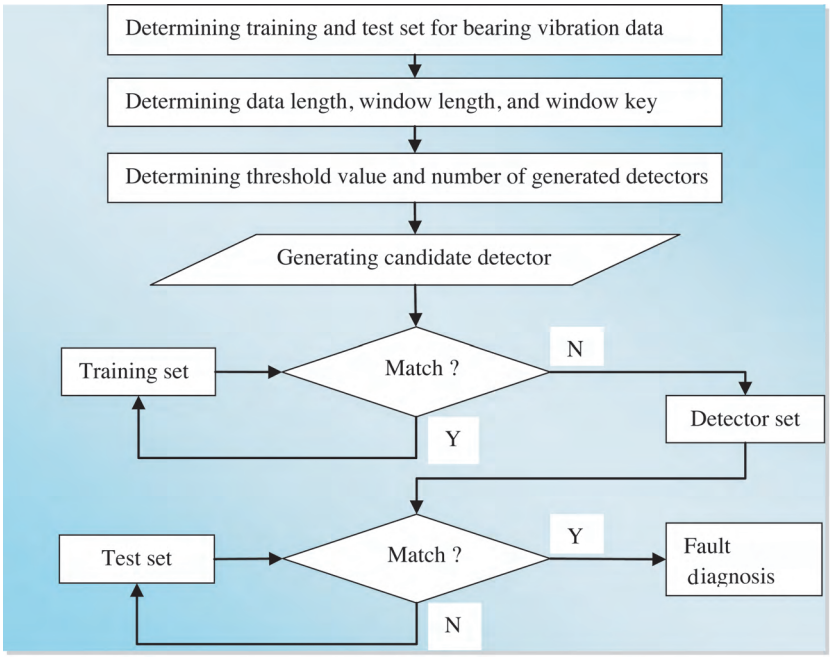

Figure 9. Flowchart of the fault detection algorithm in the time domain.

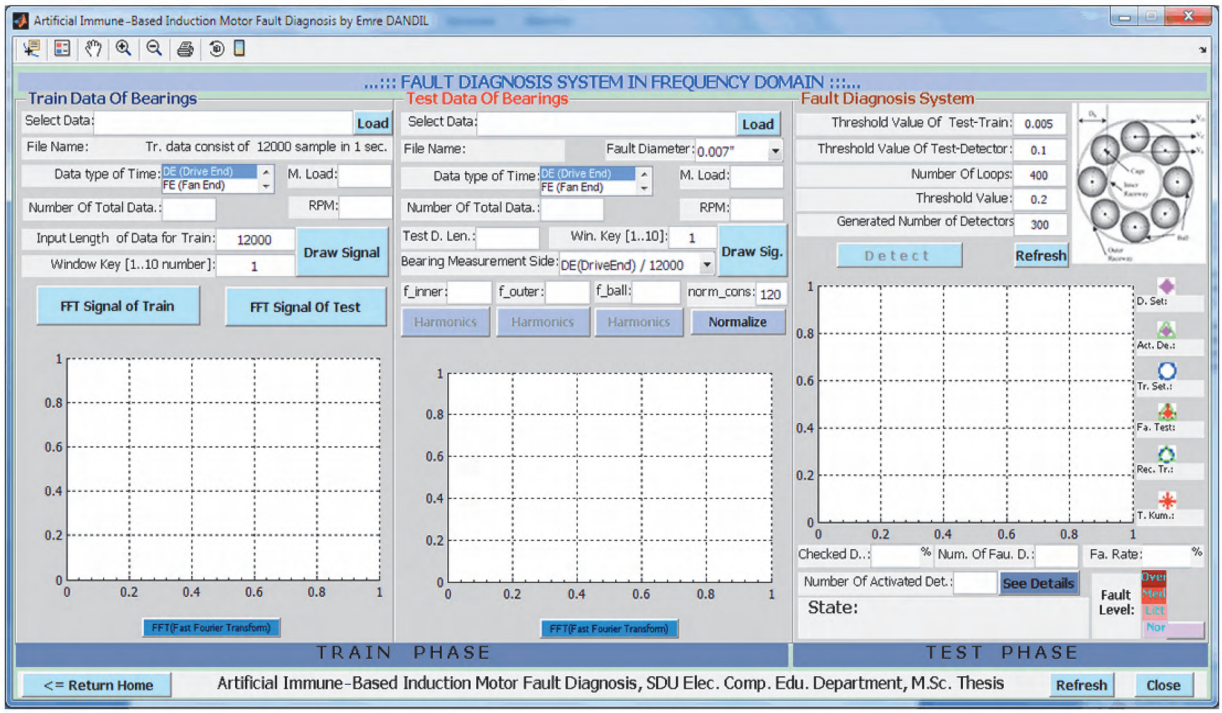

Figure 10. The fault diagnosis system in the frequency domain.

Output results and graphical analysis of the data given in Figure 12 are shown in Figure 13.

The number of activated detectors, shown in Figure 13, is 277. This gives us an indication of the fault level. The generated detectors and the frequency of activated detectors are shown in Figure 14. Here, in the

time domain, the frequency of the activated detectors indicates not only the time intervals at which the fault appears, but also the size of the fault.

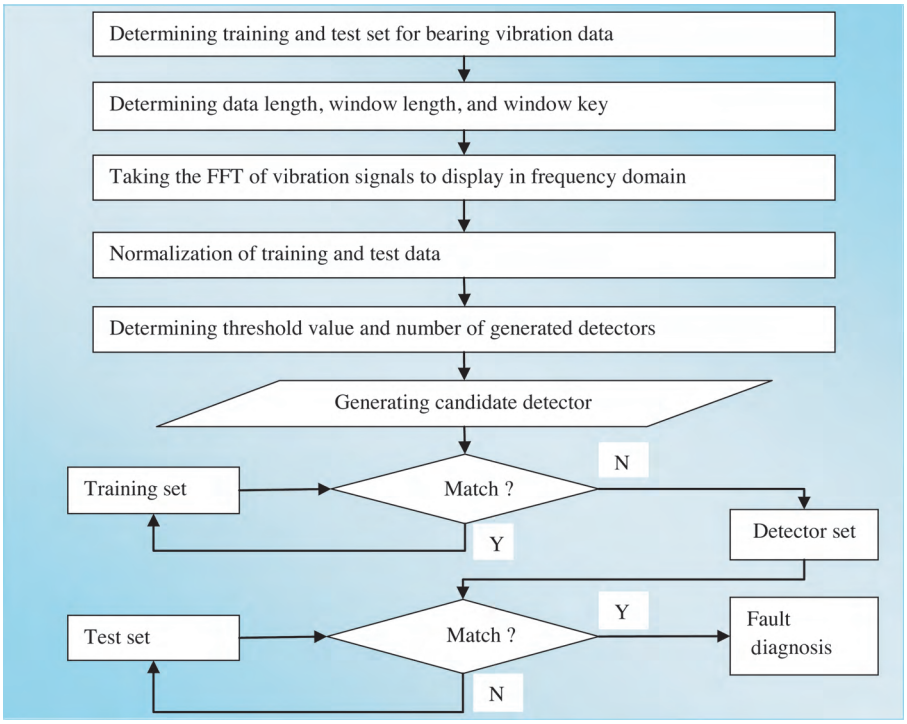

Figure 11. A flowchart of fault detection in the frequency domain.

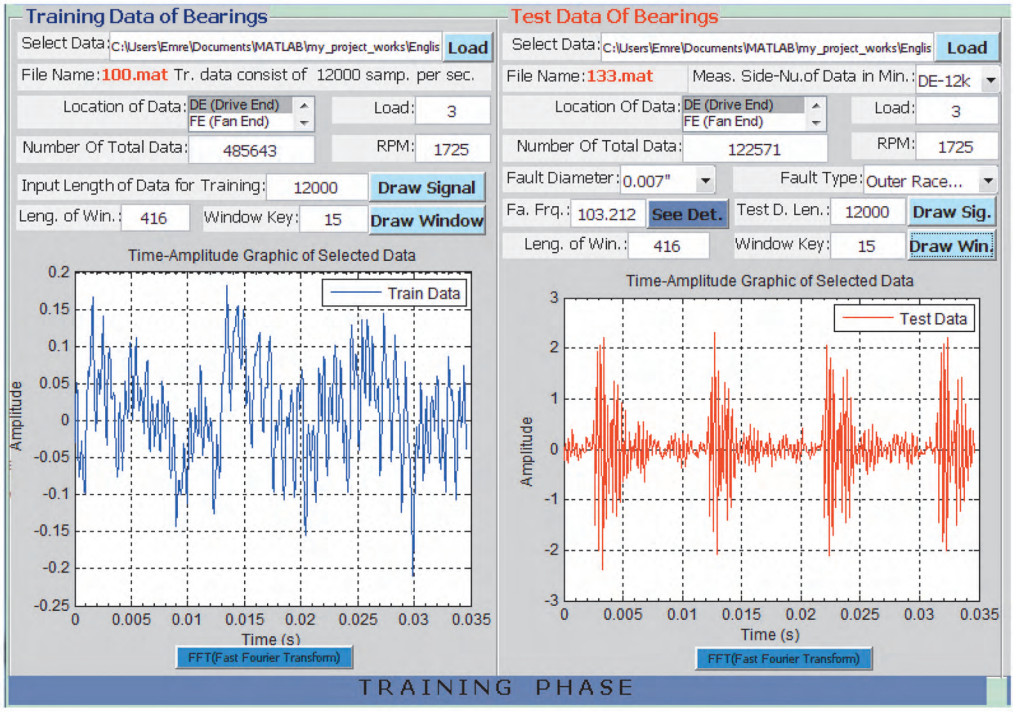

Figure 12. Training and test data for the outer race.

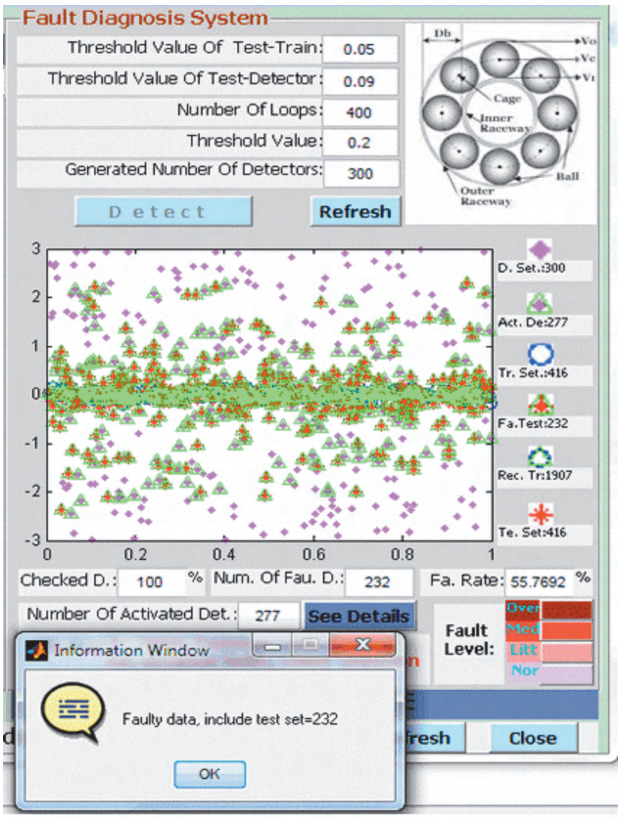

Figure 13. Results of the diagnostic software for the outer race.

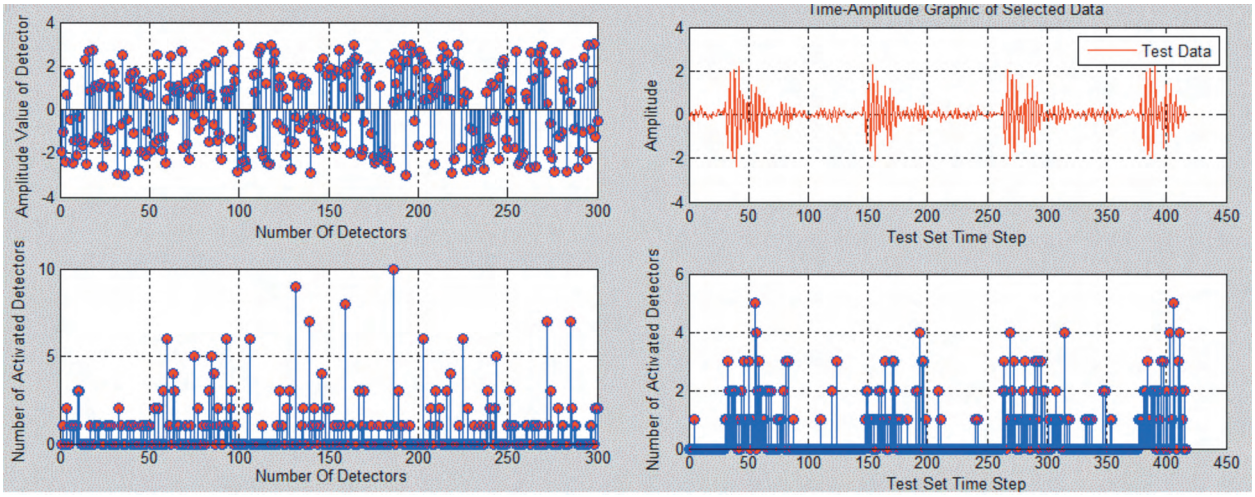

Figure 14. Number of activated detectors and time instants for the detector activation

In Figure 14, it is seen that the number of activated detectors is increasing as long as the fault level is getting worse. Moreover, in Figure 14, in the time intervals at which the highest fault level exists, there are periodical aggregations. These indicate abnormal conditions and a mean high vibration exists in the motor. Because the motor is operated at full load, amplitude changes in the vibration signals and the increment in the number of activated detectors are caused only because of the fault level, not from the load condition.

4.1.2. Diagnosis of bearing faults in the inner race

For inner race fault detection, first the training data and their details are shown, as on the left side of Figure 15, and then the test data and their details are displayed, as on the right side of Figure 15.

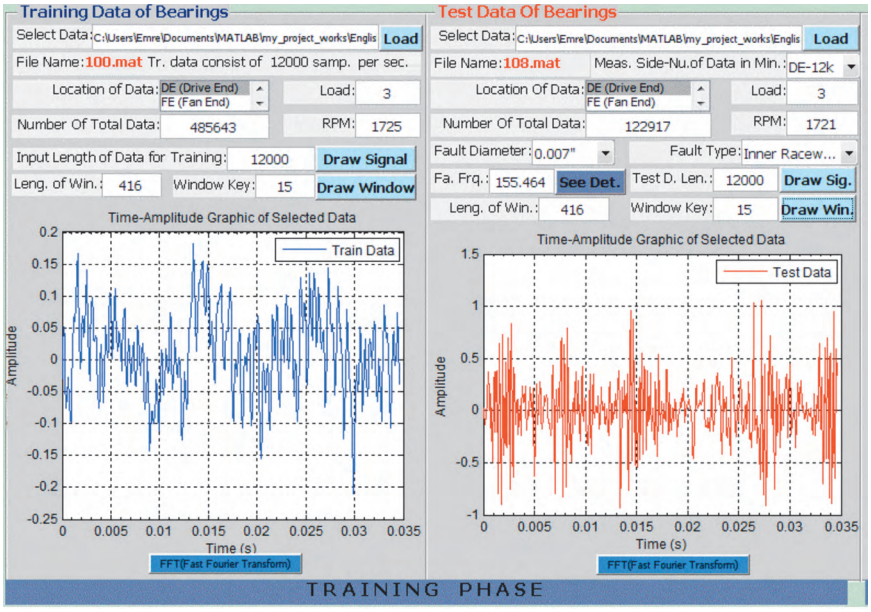

Figure 15. Training and test data for the inner race fault.

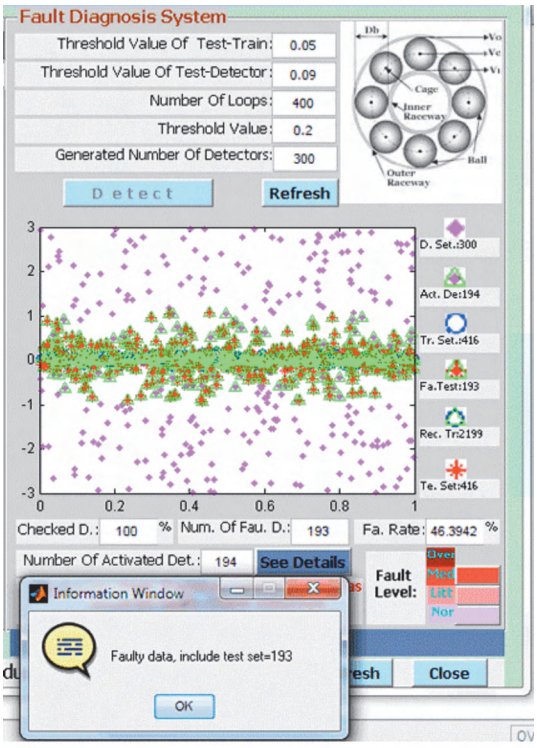

Figure 16. Results of the fault diagnostic software for the inner race.

After processing the data, the graphical and numerical results from the user interface-based fault diagnosis software are shown as in Figure 16.

Both the number and frequency of activated detectors are shown in Figure 17. Here, in the time domain, they indicate the time intervals for the fault appearance instants and fault level.

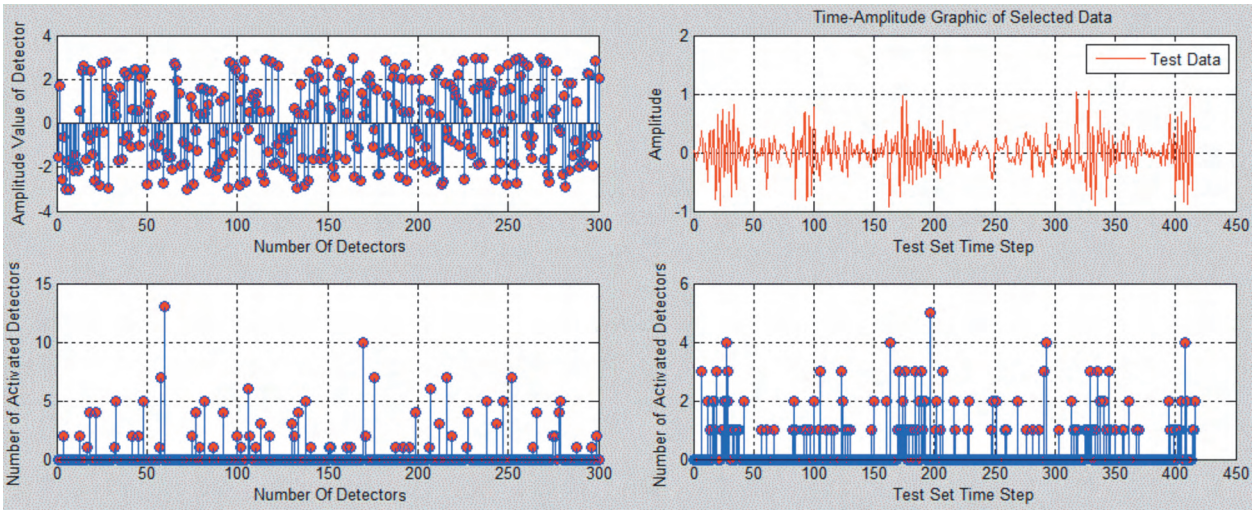

Figure 17. Number of activated detectors and time instants for the detector activation.

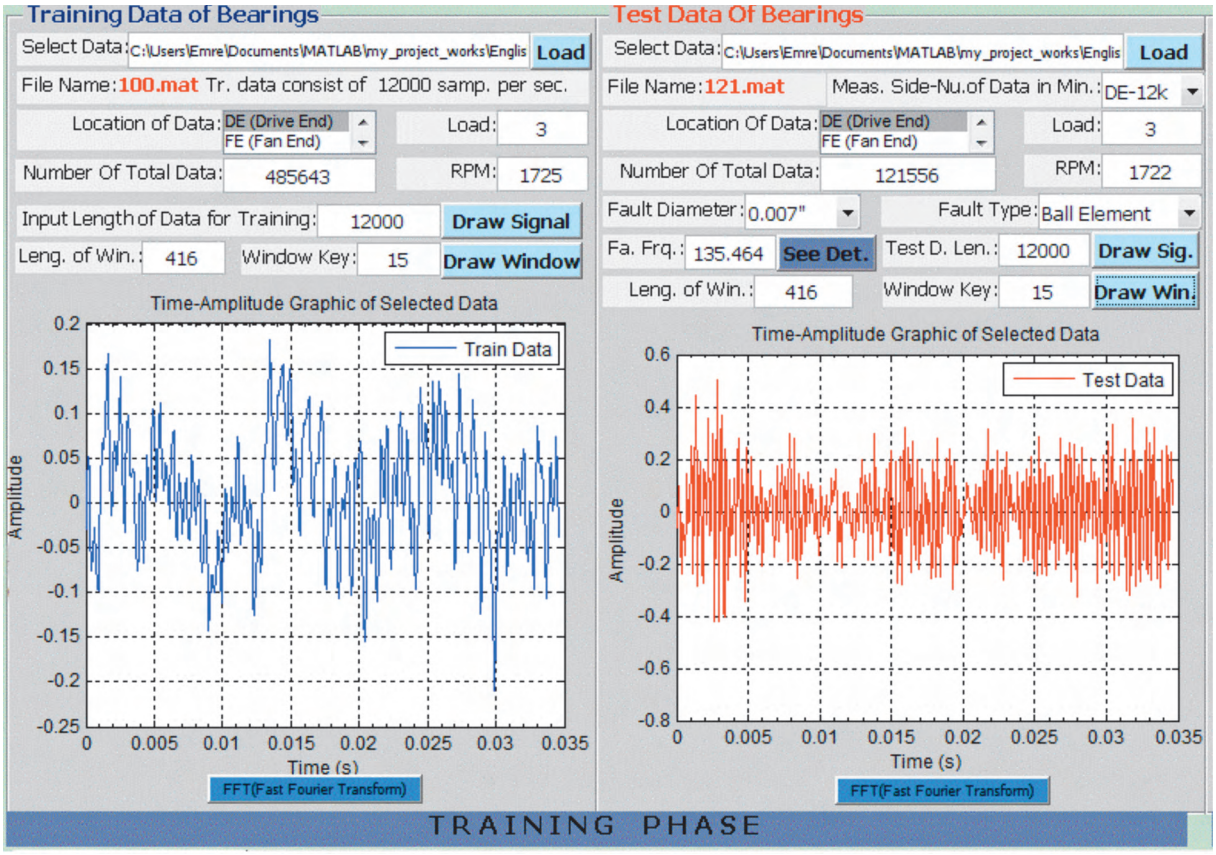

Figure 18. Training and test data for rolling element fault detection.

4.1.3. Diagnosis of bearing faults in the rolling element

For ball defect detection, the training data, test data, and their details are shown as in Figure 18. There is a minimum amount of ball defect on the bearing at the drive-end side of the motor that is running at full load.

The output of the fault diagnosis software on the graphical user interface as a graphical and numerical value is shown in Figure 19.

Both the number and the frequency of the activated detectors are shown in Figure 20. Here, in the time domain, they indicate the time intervals for the fault appearance instants and fault level.

For the time domain, the summary of the output results of the fault diagnosis software executed for different fault types, levels, loads, and locations are shown in Table 2.

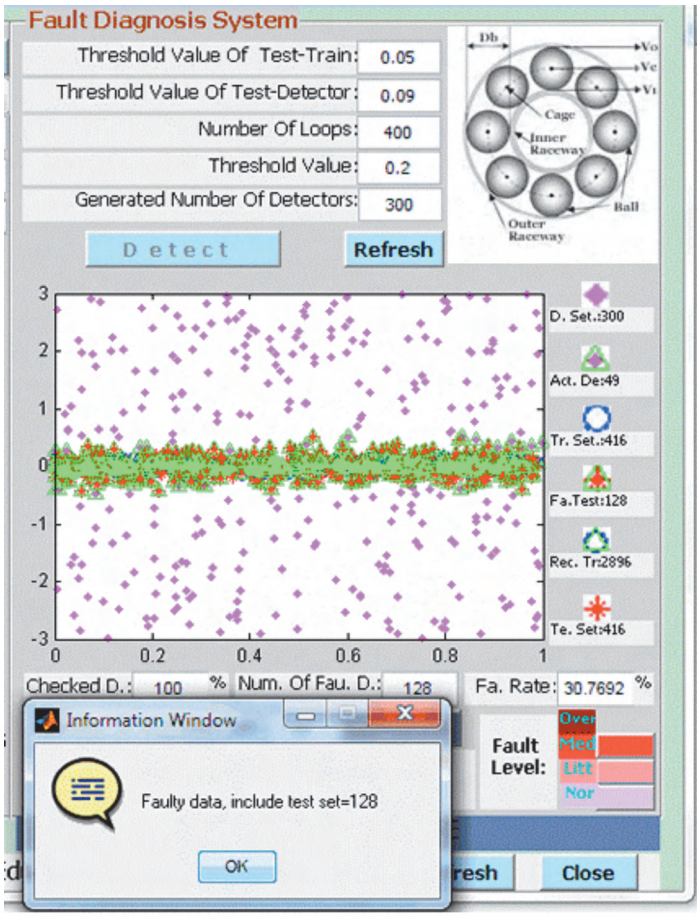

Figure 19. Results of the fault diagnostic software for the ball element.

Under different conditions, the results of the fault diagnosis shown in Table 2 are summarized as follows:

i. In rows 1, 2, 3, 4, 5, 6, and 7, changes in the motor load do not affect the fault diagnosis results because changes in the fault rate and number of activated detectors that occur at no load and full load motor conditions are close to each other.

ii. For rows 1, 2, 3, 4, 5, 6, and 7, according to the same specifications of the training and test data, because the highest fault rate and number of activated detectors are for the outer race fault, it is seen that the easiest fault detection is in the outer race fault.

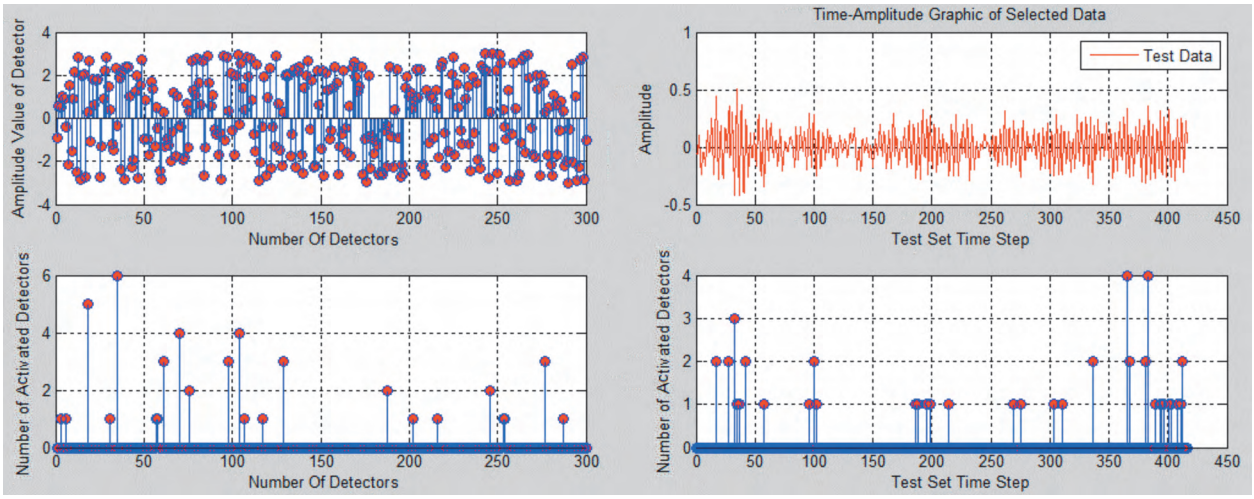

Figure 20. Number of activated detectors and time instants for the detector activation.

Table 2. Fault diagnosis results of different situations in the time domain.

Diagnosis number	Location of the bearings	Number of data	Fault diameter (cm)	Bearing fault	Load level	Speed (rpm)	Window size	Window key	Position of the accelerometer	Number of training data	Number of test data	Number of faulty data	Fault rate (%)	Number of activated detectors
1	DE	12,000	0.0534	Inner	1	1774	12,000	1	DE	185	185	158	84.41	183
2	DE	12,000	0.0356	Inner	3	1728	12,000	1	DE	185	185	162	87.57	149
3	DE	12,000	0.0356	Outer	3	1728	12,000	1	DE	285	285	228	80.00	139
4	DE	12,000	0.0356	Ball	3	1728	12,000	1	DE	215	215	173	80.47	173
5	FE	12,000	0.0178	Outer	2	1756	12,000	1	DE	330	330	269	81.52	115
6	FE	12,000	0.0178	Outer	2	1756	12,000	1	FE	330	330	305	92.42	185
7	DE	48,000	0.0178	Inner	0	1796	12,000	1	DE	180	180	122	67.78	71

iii. The window length in the fault diagnosis is defined as 416 in Table 1. This value is equal to the number of data to cover one complete cycle of motor rotation. Hence, the determination of the window length like this provides fault detection by moving windows. According to the results in rows 7, 8, 9, and 10, it is clear that changes in the window location do not affect the fault rate. This depicts that similar vibration signals are produced for each complete rotation of the motor only for the outer race fault.

iv. From the results in rows 9 and 11, extreme increments in both the number of activated detectors and the fault rate are only because of changes in the fault level.

v. According to the results in rows 2, 4, 12, and 13, under the same motor load conditions, fault type, and fault level, it is seen that fault detection is realized more effectively from the drive-end side of the motor.

vi. From the results in rows 14, 15, and 16, the best fault detection location for the outer race fault is in the load zone (clock @6:00) directly.

vii. According to the results in rows 4 and 17, it is noticed that changes in window length have little effect on the fault rate.

4.2. Results in the frequency domain

In the frequency domain, in contrast to fault detection in the time domain, only the fault related to frequency components and their harmonics are used in fault diagnosis.

4.2.1. Diagnosis of bearing fault in the inner race

For inner race fault detection, spectrums of the training and test data are shown in Figure 21. There is a clear increment in the magnitudes and an evident increase in the high frequency region of the spectrum.

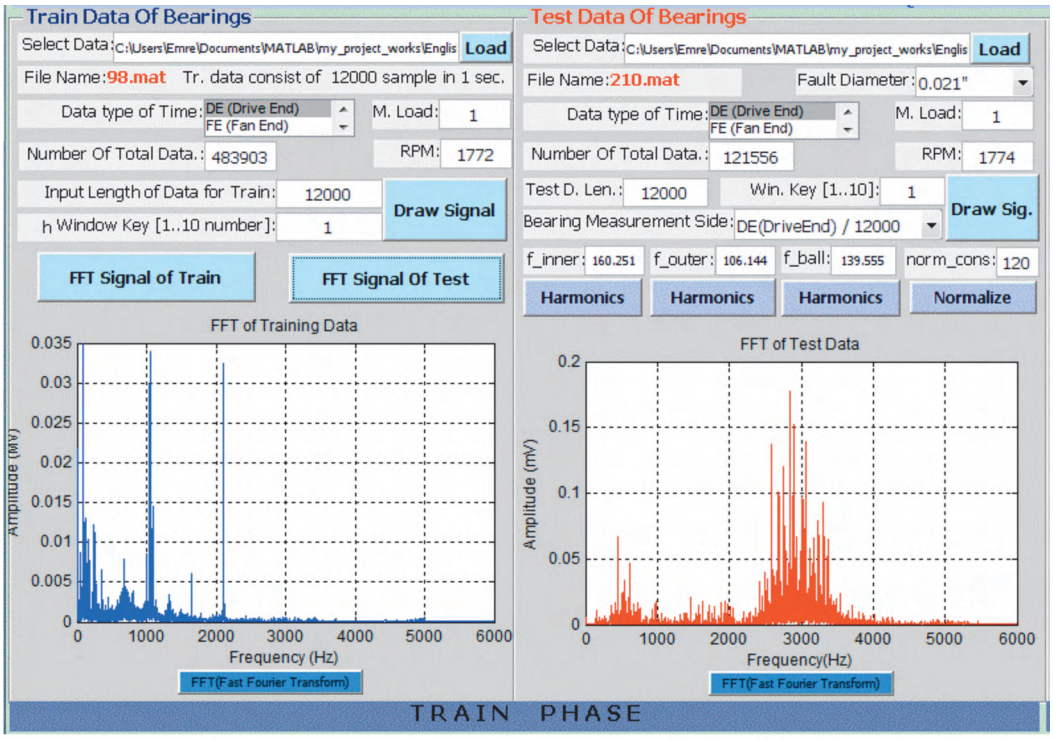

Figure 21. The whole spectrum range for the training and test data for the inner race fault.

Figure 21 shows the whole spectrum of the training and test data for the inner race fault detection. However, only the fault indicator frequency component and its harmonics are displayed after normalization, as shown in Figure 22.

Output results and graphical analysis of the data are shown in Figure 23. Here, it is seen that maximum number of detectors is activated due to the excess fault level.

The generated detectors for fault detection are shown in Figure 23. The activation frequency of these detectors and the harmonics of the activated detectors are shown in Figure 24.

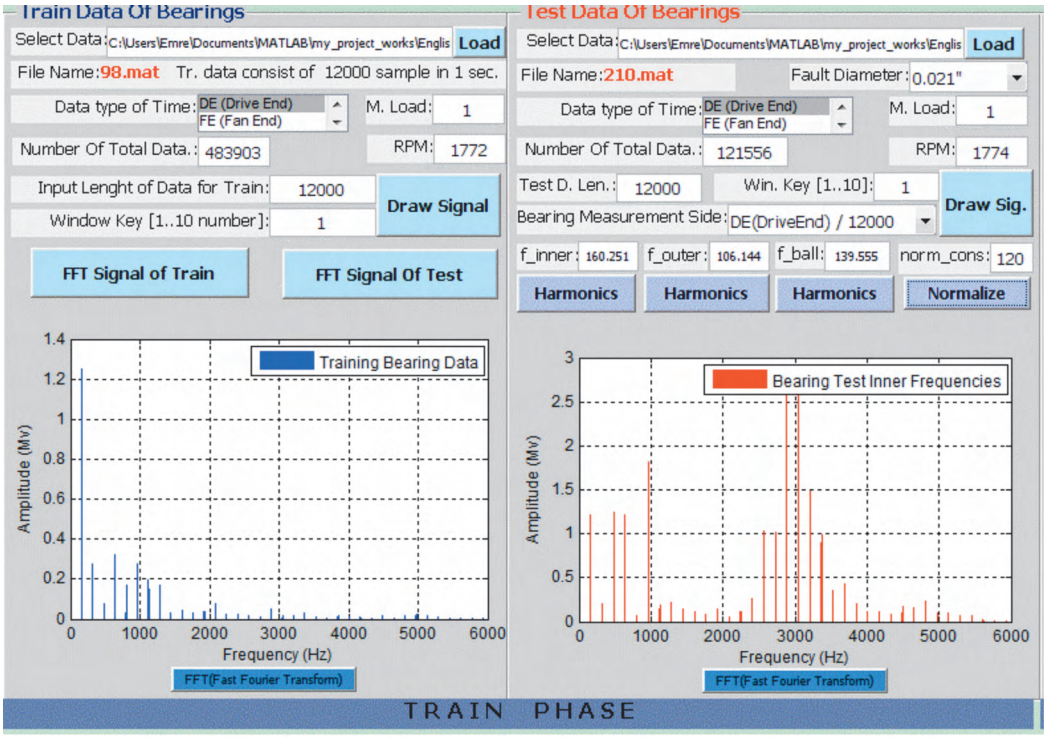

Figure 22. Decomposed and normalized spectrum of the training and test data for the inner race fault.

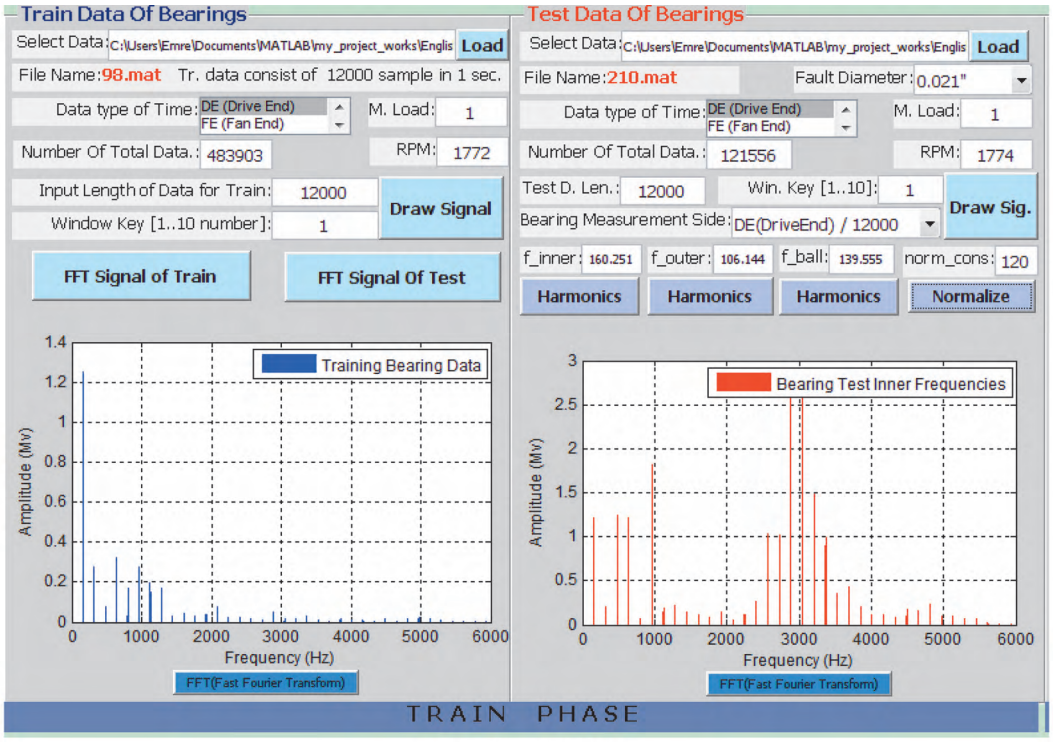

Figure 23. Results of the fault diagnostic software for the inner race.

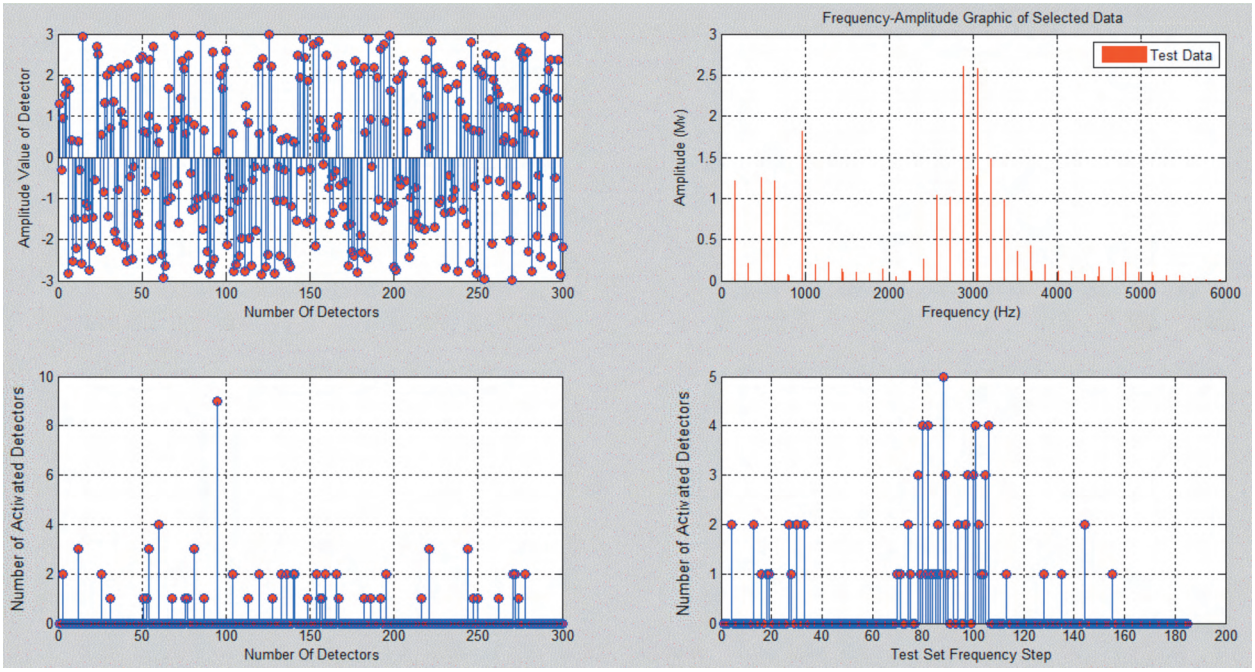

Figure 24. Number of activated detectors and number of activated detectors at which harmonics are high.

In Figure 24, it is clear that the number of activated detectors is increased with the fault level. However, from Figure 24 it is also noticed that the number of activated detectors with high-order harmonics is increased. This indicates abnormal conditions and means that high vibration occurs in the induction motor.

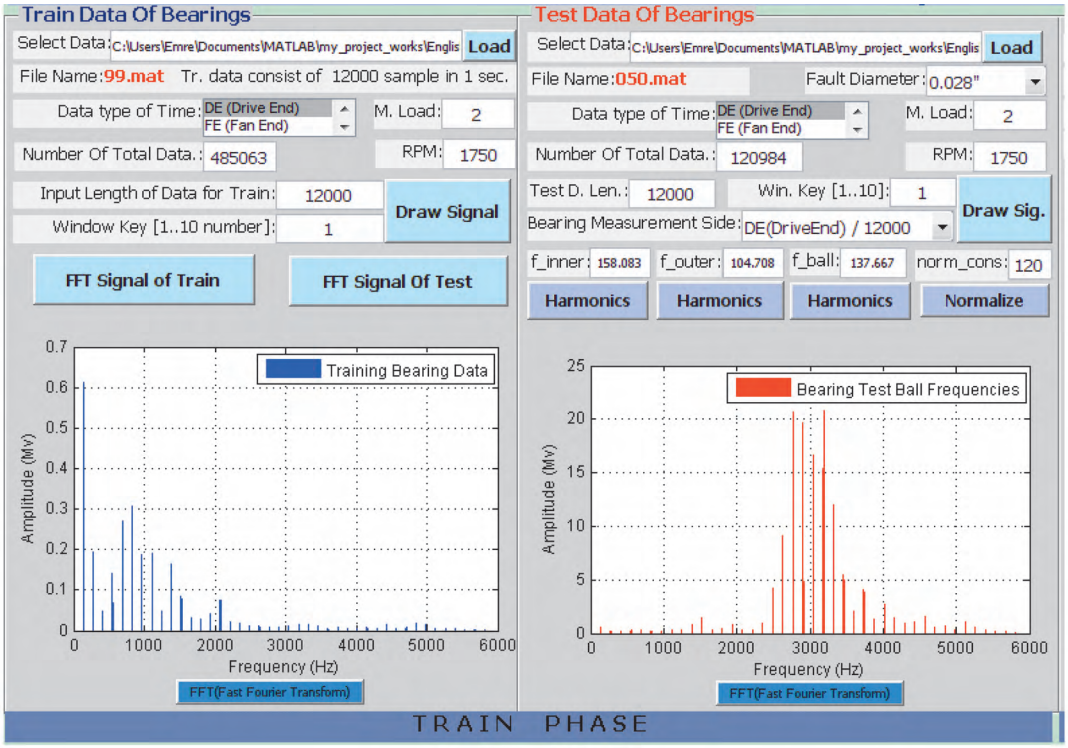

Figure 25. Decomposed and normalized spectrum of the training and test data for the outer race fault.

4.2.2. Diagnosis of bearing faults in the outer race

For outer race fault diagnosis, spectrums of the training and test data are presented in Figure 25. Here, the motor is running at full load condition and the fault diameter is approximately 0.0356 cm.

In Figure 26, for outer race fault detection, output results of the algorithm, graphical analysis, and other details are depicted.

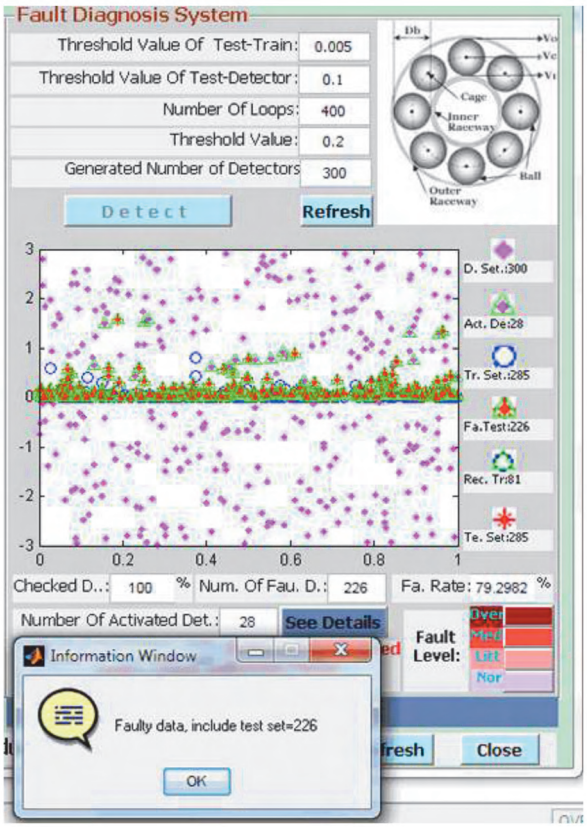

Figure 26. Results of the fault diagnostic software for the outer race.

The generated detectors for fault detection are illustrated in Figure 26, and the activation frequency of these detectors and the number of activated detectors at which harmonics are high are shown in Figure 27.

4.2.3. Diagnosis of bearing faults in the rolling element

For rolling element fault detection, the normalized and decomposed harmonics of the ball passing frequency are shown in Figure 28. In this condition, the motor is loaded above the half range and the fault diameter is about 0.0712 cm.

For rolling element fault detection, the output results of the algorithm, graphical analysis, and other details are presented in Figure 29.

The generated detectors for the fault detection are illustrated in Figure 29, and the activation frequency of these detectors and the number of activated detectors at which harmonics are high are displayed in Figure 30.

According to Table 3, the number of activated detectors in the rolling element fault is larger.

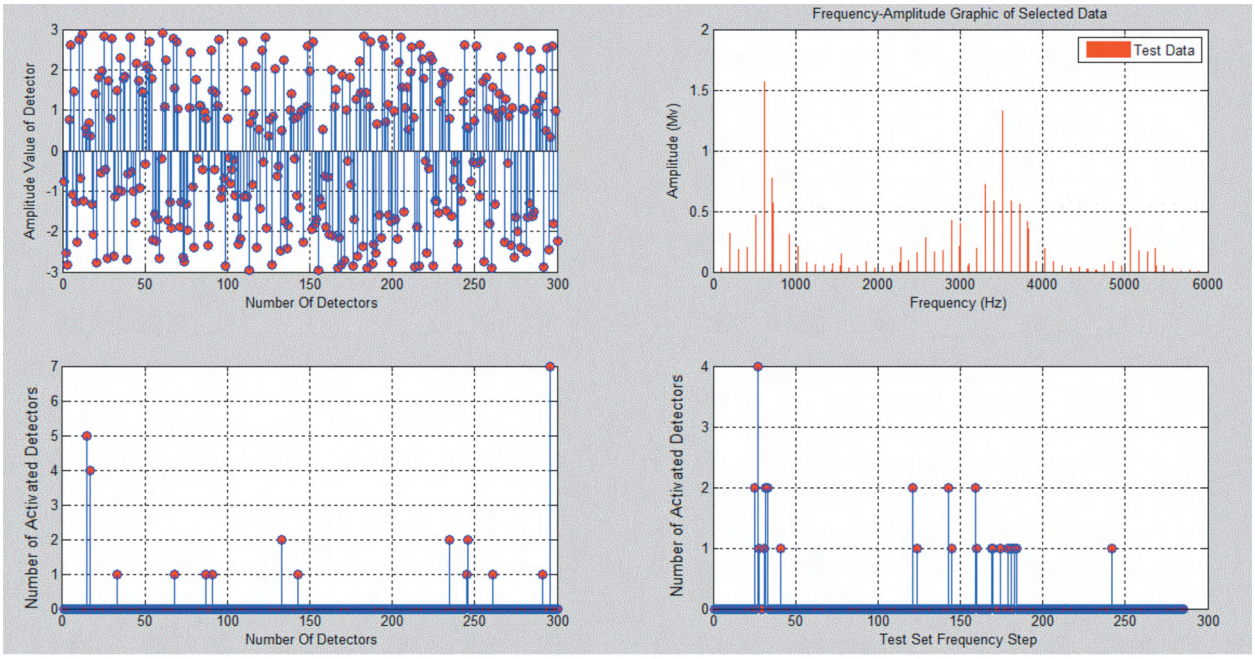

Figure 27. Number of activated detectors and number of activated detectors at which harmonics are high.

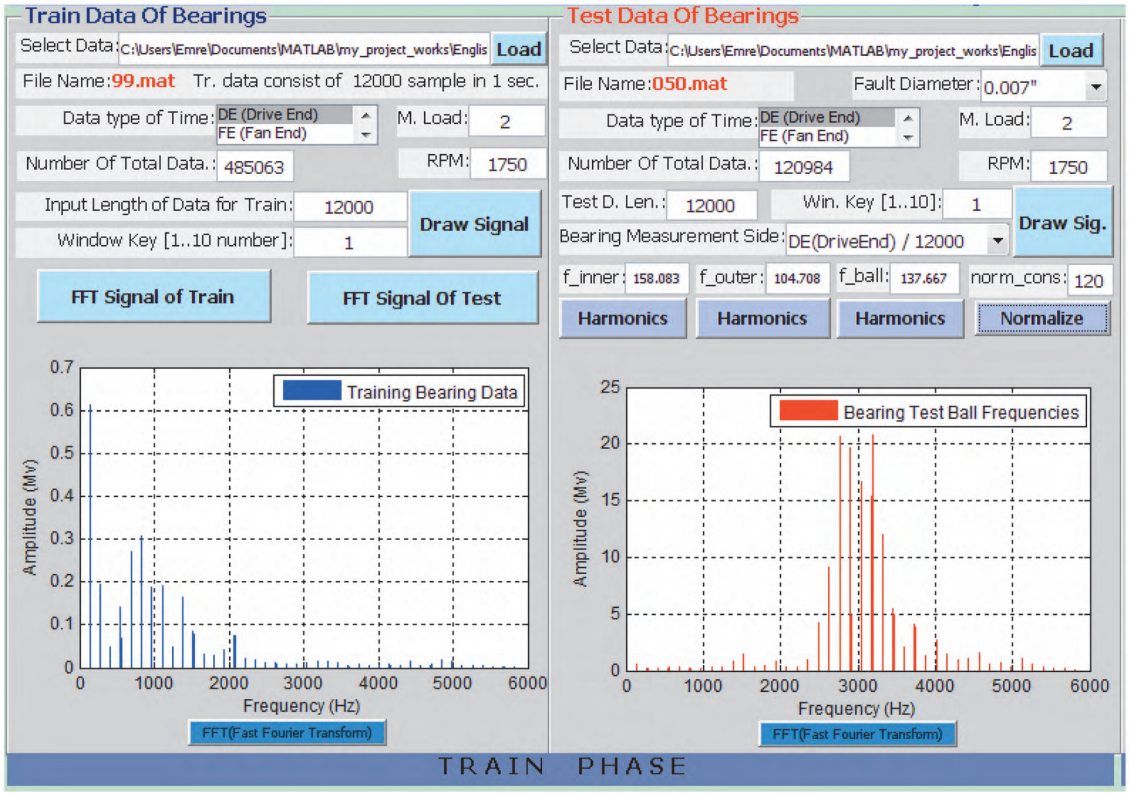

Figure 28. Decomposed and normalized spectrum of the training and test data for the rolling element fault.

For the frequency domain, the summary of the output results of the fault diagnosis software executed at different fault types, levels, loads, and locations are shown in Table 4.

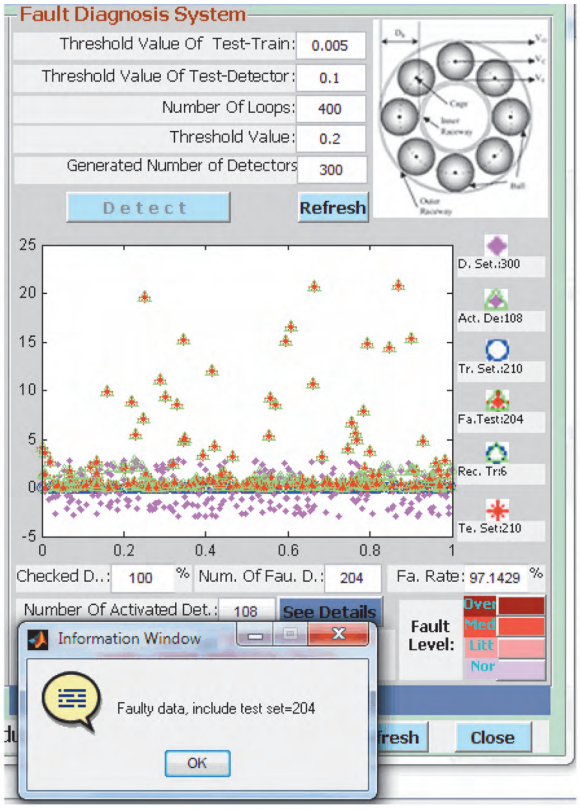

Figure 29. Results of the fault diagnostic software for the rolling element fault.

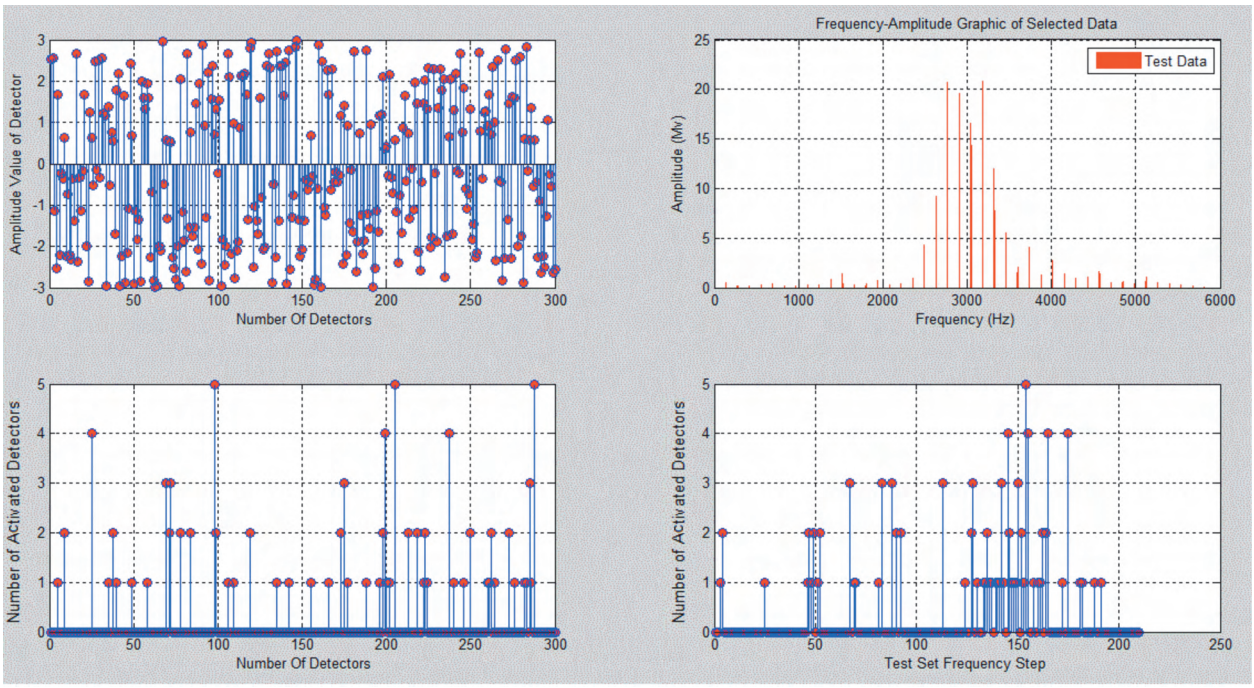

Figure 30. Number of activated detectors and number of activated detectors at which harmonics are high.

Table 3. Results in the frequency domain.

Load	Fault type	Fault diameter (cm)	Number of activated detectors	Fault rate (%)
1	Inner race	0.0534	135	85.94
3	Outer race	0.0356	124	82.10
2	Rolling element	0.0712	226	96.09

Table 4. Fault diagnosis results for different conditions in the frequency domain.

Diagnosis number	Location of the bearings	Number of data	Fault diameter (cm)	Bearing fault	Load level	Speed (rpm)	Window size	Window key	Position of the accelerometer	Number of training data	Number of test data	Number of faulty data	Fault rate (%)	Number of activated detectors
1	DE	12,000	0.0534	Inner	1	1774	12,000	1	DE	185	185	158	84.41	183
2	DE	12,000	0.0356	Inner	3	1728	12,000	1	DE	185	185	162	87.57	149
3	DE	12,000	0.0356	Outer	3	1728	12,000	1	DE	285	285	228	80.00	139
4	DE	12,000	0.0356	Ball	3	1728	12,000	1	DE	215	215	173	80.47	173
5	FE	12,000	0.0178	Outer	2	1756	12,000	1	DE	330	330	269	81.52	115
6	FE	12,000	0.0178	Outer	2	1756	12,000	1	FE	330	330	305	92.42	185
7	DE	48,000	0.0178	Inner	0	1796	12,000	1	DE	180	180	122	67.78	71

After comparison of Tables 1 and 3, it is clear that the fault rate in the frequency domain is larger than the rate in the time domain, because anomaly detection in the frequency domain is implemented directly on the related harmonics.

5. Conclusion

In this paper, bearing faults were detected by anomaly monitoring, both in the time and frequency domains. For this purpose, AIS-based graphical user interfaced software was developed. Anomaly detection was implemented by monitoring amplitude changes in the time domain and harmonics of the bearing frequencies in the frequency domain. Due to its constant location and closeness to the accelerometer, the outer race fault is the most easily determined fault type. However, the most difficult fault type to detect is the ball defect. By verification of the detection results, the motor load is seen to have very little effect on the fault. The time instants of fault occurrence and fault level are determined according to the number of activated detectors.

The fault rate given in this paper does not represent a success rate. It indicates a percentage of the number of faulty data in the given test data. This rate indicates whether a fault exists in the data array or not. According to the obtained results in this paper, the inner race, outer race, and rolling element faults in the bearings have been determined with certainty.

The number of faulty data in the test part has been given in percentage form. Increments in the fault rate

are directly proportional to the number of activated detectors. The amount of activated detectors represents the fault level and also provides the location of the anomalies in time steps. In addition, an increase in the fault diameter raises the fault rate.

The main contributions and advantages of the implemented fault detection system are as follows:

- Diagnosis is implemented both in the time and the frequency domain.
- The fault level is determined by the increasing number of activated detectors.
- Fault occurrence instants are found by monitoring how frequently detectors are activated.
- There are few published papers about fault diagnosis by AIS.
- The developed software is a graphical user interface that is adaptive and versatile for any other signal usage.

Multifault classification by AIS in either motors or pumps is intended for future studies.

References

[1] S. Abbasion, A. Rafsanjani, A. Farshidianfar, N. Irani, "Rolling element bearings multi-fault classification based on the wavelet denoising and support vector machine", Mechanical Systems and Signal Processing, Vol. 21, pp. 2933–2945, 2007.

[2] X. Gao, S. Ovaska, "Soft computing methods in motor fault diagnosis", Applied Soft Computing, Vol. 1, pp. 73–81, 2001.

[3] E. Ayaz, S. Şeker, "İleri işaret işleme yöntemleri ile elektrik motorlarında rulman arıza tanısı", İstanbul Teknik Üniversitesi Mühendislik Dergisi, Vol. 1, pp. 23–34, 2002.

[4] S. Orhan, H. Arslan, N. Aktürk, "Titreşim analiziyle rulman arızalarının belirlenmesi", Gazi Üniversitesi Mühendislik Mimarlık Fakültesi Dergisi, Vol. 18, pp. 39–48, 2003.

[5] O. Özgönenel, T. Yalçın, "A complete motor protection algorithm based on PCA and ANN: a real time study", Turkish Journal of Electrical Engineering & Computer Sciences, Vol. 19, pp. 317–334, 2011.

[6] Z. Kıral, H. Karagülle, "Rulmanlı yatak geometrilerinde bölgesel hata adedinin titreşim sinyalleri üzerindeki etkisinin zaman ve frekans ortamlarında incelenmesi", 12. Ulusal Makina Teorisi Sempozyumu, Erciyes University, pp. 1–12, 2005.

[7] P.J. Costa Branco, J.A. Dente, R.V. Mendes, "Using immunology principles for fault detections", IEEE Transactions on Industrial Electronics, Vol. 50, pp. 362–372, 2003.

[8] B. Alataş, İ. Aydın, E. Akın, "Asenkron motorların hata teşhisinde yapay bağışıklık sistemi yaklaşımı", II. Mühendislik Bilimleri Genç Araştırmacıları Kongresi, pp. 76–85, 2005.

[9] İ. Aydın, M. Karaköse, E. Akın, "Artificial immune based support vector machine algorithm for fault diagnosis of induction motors", International Aegean Conference on Electrical Machines and Power Electronics, pp. 217–221, 2007.

[10] F. Duan, M. Lei, J. Li, Y. Tian, "A motor fault diagnosis method based on immune mechanism", IEEE Computer Society Workshop on Intelligent Information Technology Application, pp. 152–160, 2007.

[11] İ. Aydın, M. Karaköse, E. Akın, "Genetik algoritma kullanan yapay bağışıklık sistem tabanlı arıza teşhis modeli", Dokuz Eylül Üniversitesi Mühendislik Fakültesi Fen ve Mühendislik Dergisi, Vol. 11, pp. 57–72, 2009.

[12] Z. Gan, M.B. Zhao, T.W.S. Chow, "Induction machine fault detection using clone selection programming", Expert Systems with Application, Vol. 36, pp. 8000–8012, 2009.

[13] J.F. Martins, P.J. Costa Branco, A.J. Pires, J.A. Dente, "Fault detection using immune-based systems and formal language algorithms", Proceedings of the 39th IEEE Conference on Decision and Control, Vol. 3, pp. 2633–2638, 2009.

[14] C.A. Laurentys, G. Ronacher, Y.M. Palhares, W.M. Caminhas, "Design of an artificial immune system for fault detection: a negative selection approach", Expert Systems with Applications, Vol. 37, pp. 5507–5513, 2010.

[15] I. Aydin, M. Karakose, E. Akin, "Chaotic-based hybrid negative selection algorithm and its applications in fault and anomaly detection", Expert Systems with Applications, Vol. 37, pp. 5285–5294, 2010.

[16] Case Western Reserve University Bearing Data Center Website. http://csegroups.case.edu/bearingdatacenter/pages/welcome-case-western-reserve-university-bearing-data-center-website. Access Date: 05.02.2010.

[17] H. Ocak, K.A. Loparo, "Estimation of the running speed and bearing defect frequencies of an induction motor from vibration data", Mechanical Systems and Signal Processing, Vol. 18, pp. 515–533, 2004.

[18] I. Aydin, M. Karakose, E. Akin, "Artificial immune inspired fault detection algorithm based on fuzzy clustering and genetic algorithm", IEEE International Conference on Computational Intelligence for Measurement Systems and Applications, pp. 93–98, 2008.

[19] L.N. de Castro, J. Timmis, Artificial Immune Systems: A New Computational Intelligence Approach, London, Springer-Verlag, 2002.

[20] D. Dasgupta, S. Forrest, "Novelty detection in time series data using ideas from immunology", 5th International Conference on Intelligent Systems, pp. 19–21, 1996.

[21] S. Forrest, A.S. Perelson, L. Allen, R. Cherukuri, "Self-nonself discrimination in a computer", Proceedings of the IEEE Symposium on Research in Security and Privacy, pp. 202–212, 1994.

[22] D. Dasgupta, N.S. Majumdar, "Anomaly detection in multidimensional data using negative selection algorithm", Proceedings of the Congress on Evolutionary Computation, 2002.